JOURNAL OF AIRCRAFT
Vol. 40, No. 1, January–February 2003

Effects of Sweep on Active Separation Control at High Reynolds Numbers

Avi Seifert*
Tel-Aviv University, 69978 Ramat Aviv, Israel
and
LaTunia G. Pack†
NASA Langley Research Center, Hampton, Virginia 23681

This paper explores the effects of mild sweep on active separation control at high Reynolds numbers and incompressible Mach numbers. The model, which was tested in a cryogenic pressurized wind tunnel, simulates the upper surface of a 20% thick Glauert–Goldschmied type airfoil at zero angle of attack. The boundary-layer flow is turbulent because the tunnel side-wall boundary layer flows over the model, eliminating laminar-turbulent transition from the problem. Without control the flow separates at the highly convex area, and a large turbulent separation bubble is formed at the lee side of the model. Periodic excitation and steady mass transfer were applied to eliminate the separation bubble gradually. During the test, the Reynolds numbers ranged from 7×10^6 to 26×10^6, and the Mach numbers were 0.2 and 0.25. The test sweep angles were 0 and 30 deg. It was found that the excitation must be introduced slightly upstream of the separation region regardless of the sweep angle at low Mach numbers, as in the two-dimensional flow. The conventional swept flow scaling is valid for controlled, fully and even partially attached flow, but different scaling is required for the separated three-dimensional flow. The effectiveness of the active control is not reduced by mild sweep, and the effective frequencies do not change.

Nomenclature

C_{dp} = pressure drag coefficient
C_m = moment coefficient
C_n = normal force coefficient
C_p = wall pressure coefficient, $\equiv (P - P_S)/q$
C_μ = combined blowing momentum coefficient, $\equiv (c_\mu; \langle c_\mu \rangle)$
c = model chord
c_μ = steady blowing momentum coefficient, $\equiv J/cq$
$\langle c_\mu \rangle$ = oscillatory blowing momentum coefficient, $\equiv \langle J' \rangle/cq$
F^+ = reduced frequency, $\equiv (f x_{sp})/U_\infty$
f = oscillation frequency, Hz
h = slot height or width
J = momentum at slot exit, $\equiv \rho h U_j^2$
M = Mach number
P = pressure
q = freestream dynamic pressure, $\equiv 1/2 \rho U_\infty^2$
R_c = chord Reynolds number, $\equiv U_\infty c/\nu$
T = temperature
U, u = average and fluctuating streamwise velocity
w = fluctuating spanwise velocity
X_{sp} = distance from baseline separation to reattachment
x/c = normalized streamwise location
z = spanwise location
Λ = sweep angle, deg
ν = kinematic viscosity
ρ = density
$\langle\ \rangle$ = phase-locked values

Subscripts

d = derectified hot-wire data
j = conditions at blowing slot
R = reattachment
S = separation
$2D$ = two-dimensional
$3D$ = three-dimensional
∞ = freestream conditions

Superscript

$'$ = rms of fluctuating value

Received 24 January 2002; revision received 3 September 2002; accepted for publication 6 September 2002.

*Senior Lecturer, Department of Fluid Mechanics and Heat Transfer, Faculty of Engineering. Associate Fellow AIAA.
†Research Engineer, Flow Physics and Control Branch. Member AIAA.

I. Introduction

BOUNDARY-LAYER-CONTROL (BLC) research dates back to the turn of the 20th century (e.g., Prandtl, in Ref. 1). However, low efficiency, complexity, and maintenance difficulties prevented the utilization of laboratory proven BLC techniques, such as blowing or suction. Forced oscillations superimposed on a mean flow that is on the verge of separating were previously found to be very effective in delaying turbulent boundary-layer separation.[2] Experiments performed on various existing airfoils at low and high Reynolds numbers[3–5] demonstrated that even if the flow is not fully attached the lift could be significantly enhanced by the introduction of periodic excitation into the separated shear layer. This is achieved by exciting the flow at frequencies that generate 2–4 spanwise coherent vortices over the length of the separated region (i.e., $F^+ \approx 1$). The addition of periodic excitation into a separating turbulent boundary layer increases the momentum transfer across the shear layer, enhancing its resistance to separation under adverse pressure gradient. The technique was also demonstrated at high-Reynolds-number compressible speeds.[6–8] Though demonstrated experimentally, active separation control using periodic excitation is still a challenge for numerical simulation, moreover design tools for practical Reynolds numbers are not available.

A multidisciplinary design optimization process, using active BLC, should enable simplified high-lift systems, thicker airfoils that will allow lighter structures and greater internal volume, shorter aft bodies, size reduction, and even elimination of conventional control surfaces. The resulting systems should be simpler, cheaper, more efficient, and reliable than traditional ones, while maintaining performance.[9] Existing design tools are capable of reproducing

steady flows, including steady mass transfer. However, the inclusion of unsteady BLC effects into computational fluid dynamics (CFD) tools has not been performed. The development of a proper three-dimensional CFD design tool is dependent on the availability of a comprehensive database at relevant conditions (i.e., flight Reynolds numbers) to allow its validation.

The present experiment is aimed at improving our understanding of controlling three-dimensional separated flows at flight Reynolds numbers and providing a comprehensive database for validation of unsteady three-dimensional CFD design tools. Specifically we are exploring the effects of sweep and location for introduction of the control input. Previous publications presented some of the experimental results for incompressible[7] and compressible[8] two-dimensional flow over the same model.

Sweep and compressibility are associated in the sense that sweep was initially introduced in order to reduce the effective wing thickness ratio and therefore delay the appearance of shock waves to higher freestream Mach numbers. The importance of separation control over three-dimensional configurations stems from the need to optimize high-lift systems of swept wing airplanes as well as other three-dimensional flows. Although two-dimensional flow is relatively easy to establish and analyze, quasi-two-dimensional swept flow or infinitely swept flow is extremely complicated to duplicate and essentially impossible in the presence of separation. Presently we study the effects of active separation control by rotating the model to a mild sweep of 30 deg and comparing the results to those obtained in the absence of sweep.

Section II of this paper provides a brief description of the experimental setup. Section III presents the experimental results, initially of the baseline flow and thereafter those of the controlled flow.

II. Description of the Experiment

A. Overview

The two-dimensional setup of the experiment was described in detail in previous publications,[7,8] where the two-dimensional data were presented and discussed. Here, the three-dimensional experimental setup and results will be presented and discussed. Therefore, only essential details that distinguish the current experiment from the previous will be repeated here.

B. "Hump" Model

The model simulates the upper surface of a 20% thick, modified Glauert–Goldschmied type airfoil. The original airfoil[10,11] was designed to allow a long fetch of laminar flow, followed by a severe adverse pressure gradient and a suction slot to prevent boundary-layer separation. This type of airfoil should be extremely effective from a structural point of view (because it has a large thickness ratio), allowing a large internal volume and also effective aerodynamic performance with flow control. The Glauert–Glas II airfoil[11,12] was wind tunnel tested and flight proven.[13] In the current test only the upper surface of the modified airfoil (Fig. 1) was installed on the right-side tunnel turntable of the wind tunnel (Fig. 2). The reference chord is 200 mm. The original location of the airfoil leading edge is defined as the reference leading edge (LE; Figs. 3). This area was faired smoothly from $x/c = -0.05$ to 0.05 in order to eliminate slope

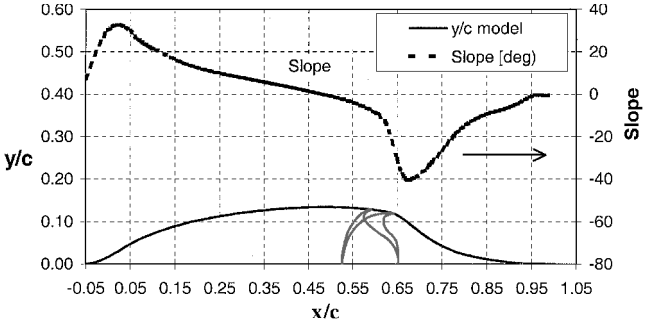

Fig. 1 Cross section of the "Hump" model, showing the alternative slots at $x/c = 0.59$ and 0.64, actuator cavity and surface slope.

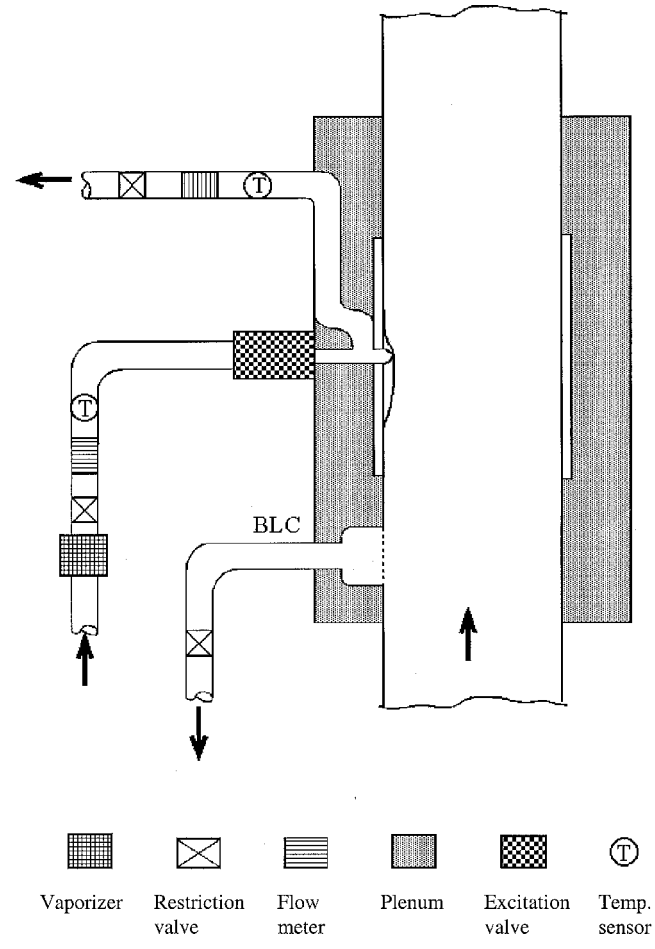

Fig. 2 Top view of the experimental setup in the 0.3-m transonic cryogenic wind tunnel. The model is shown on the left-side turntable. BLC denotes side-wall boundary-layer removal system.

discontinuity. Two alternative excitation slot locations are available: $x/c = 0.59$ and 0.64. The slots were about 0.25% chord wide (0.50 ± 0.05 mm) and allowed an almost tangential downstream introduction of steady or oscillatory momentum (Fig. 1; the slots were machined at an angle of 30 deg to the airfoil surface). The floor and ceiling boundary layers did not affect the spanwise uniformity of the flow over the model that was installed on the sidewall because of the use of a pair of end plates (vertical thick lines on Figs. 3). The gap between the end plates and the tunnel walls was 12.7 mm, which was deemed sufficient, based on the available wind-tunnel boundary-layer data.[7,14] The tunnel cross-sectional blockage caused by the model and end plates was 0.0836. The model allows testing at 0- and 30-deg sweep. The swept configuration was achieved by removing certain parts of the model, rotating the turntable on which the model was installed by 30 deg and placing alternative parts of the model and an alternative set of end plates (as shown in Fig. 3b). The pressure tap locations are also shown in Figs. 3. The streamwise row contains 34 taps, aligned at about 20 deg with the freestream direction (at zero sweep) that is also used for the 30-deg swept configuration. Three spanwise rows, of nine pressure taps each, are located at $x/c = 0$, 0.49, and 0.95. The pressure taps are spaced every 25.4 mm ($0.127c$) and cover half the chord length on each side of the centerline. The swept configuration contains two additional taps on the forward upstream end (Fig. 3b). The internal diameter of all pressure tap orifices was 0.254 mm. The model was also instrumented with 12 unsteady pressure transducers (indicated by $\times$ symbols on Figs. 3). The transducers are installed under the model surface inside small volume cavities. The cavities are connected to the surface of the model by tiny orifices, 0.254 mm in diameter. The effect of this installation on the frequency response of the unsteady pressure transducers is complex. Therefore, only the flat range of the transducers frequency response (up to about 2 kHz) is considered. A

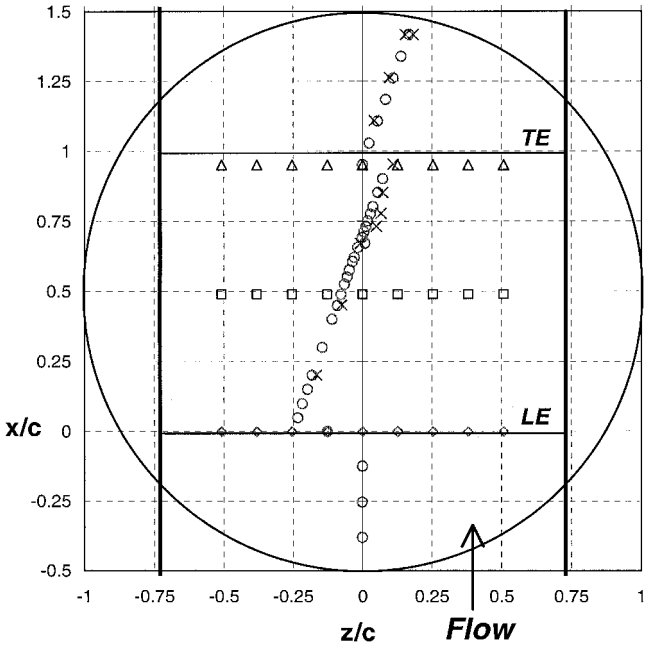

Fig. 3a Top view of the unswept model. The vertical ——, indicate the location of the end plates.

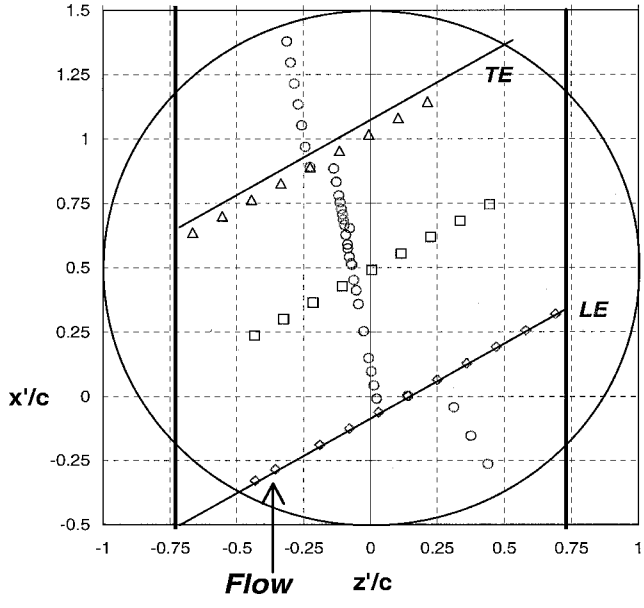

Fig. 3b Top view of the swept model. The vertical ——, indicate the end plates.

comprehensive bench-top calibration and occasional in situ testing by a piezoelectric actuator were conducted to validate the sensors' performance. In addition, one transducer was flush mounted near the trailing edge of the turntable next to a recessed pressure transducer, and their readings are compared. The full scale of the unsteady pressure transducers is 10 psid. They were referenced to the static wall pressures immediately next to the orifice locations or to the wind-tunnel plenum pressure in order to maintain optimal resolution even at static pressures that exceed the transducer's range. One unsteady pressure transducer was installed inside the model cavity, midway between the end plates and about 30 mm from the slot exit. It is used to monitor the cavity pressure oscillations in the wind tunnel and to correlate the wind-tunnel data with the bench-top calibration of the slot exit velocity vs the imposed cavity pressure oscillations.

C. 0.3-Meter Transonic Cryogenic Wind Tunnel

The experiment was conducted in the 0.3-meter Transonic Cryogenic Wind Tunnel at the NASA Langley Research Center. It is a closed-loop, fan-driven tunnel with a test cross section of 0.33 by 0.33 m. Gaseous nitrogen is the test medium. The tunnel operates at stagnation pressures ranging from 1.2 to 6 bars and total temperatures from 78 up to 327 K.[15,16] A fully automatic control system maintains the test conditions, providing a high level of repeatability. The floor and ceiling of the tunnel were slightly diverged near the model to reduce blockage resulting from boundary-layer growth on the test-section walls. The tunnel side walls are parallel, so that no divergence is possible in the direction normal to the model surface. In certain runs a turntable that was instrumented with static pressure orifices was placed opposite the test model in order to evaluate wall interference. A schematic description of the experimental setup in the wind tunnel is given in Fig. 2.

D. Oscillatory Blowing System

The Oscillatory Blowing System is capable of generating any desired combination of steady and periodic momentum transfer between the cavity inside the model and the external flow. More details can be found in Refs. 5–8.

E. Bench-Top Experiments

A bench-top calibration was performed in order to correlate the fluctuating slot velocities ($u'_{j,d}$) with the cavity pressure fluctuations (p'_c). This calibration was performed for the $x/c = 0.59$ and 0.64 slots and covered the entire frequency range and most of the normalized amplitude $(p'/\rho)_c$ range that was used in the cryogenic wind-tunnel tests. The frequency response of the present excitation system (oscillatory blowing valve-manifold-cavity) is significantly simpler than the one used previously.[5] This allows the generation of a single correlation between $u'_{j,d}$ and $(p'/\rho)_c$ for each slot calibration. The slot width changed by as much as $\pm 10\%$ (0.05 mm) between different runs because of the modular nature of the model and also as a result of cryogenic cycling. This is accounted for in the uncertainty level of $\langle c_\mu \rangle$ (i.e., $\pm 25\%$). More details on the slot calibration are given in Refs. 5–8. Note that the preceding slot calibration is not affected by sweep.

F. Experimental Uncertainty

Most of the experiments were conducted at cryogenic pressurized conditions (about 100 K), close to the lower limit of the tunnel capability. Most of the data were obtained with separated flow regions on the model. Table 1 contains the relevant information regarding experimental uncertainty. These values were calculated using ± 3 standard deviations of the various experimental conditions and calculated parameters (including repeated runs). All of the test instruments were operated with valid calibrations.

The uncertainty of the calculated aerodynamic parameters are listed in Table 2 (in absolute values and related to flow condition on the model).

Table 1 Uncertainty of flow and control parameters, % of full scale unless otherwise noted

Item	Uncertainty (of full scale)	Full scale and condition
Slot width	10%	0.5 mm
Static temperature	0.3%	300 K
Static pressure	0.25%	77 psi
R_c	1%	$M > 0.2$
M	2%	Local values
F^+	2%	2
c_μ	0.01 or 10%	The larger
$\langle c_\mu \rangle$	25%	Local values
f	0.3%	800 Hz
C_p	1%	$M < 0.3$
$C_{p,\mathrm{rms}}$	15%	$M < 0.3$

Table 2 Uncertainty of aerodynamic parameters

Parameter	Baseline	Controlled
C_n	0.010	0.015
C_{dp}	0.0005	0.0010
C_m	0.005	0.010

G. Experimental Conditions

The experiments were conducted at Mach numbers of 0.20 and 0.25 and chord Reynolds numbers ranging from 7.0×10^6 to 26.0×10^6.

III. Results

Overview

The results presented in this part of the paper are divided into two sections. The first section describes the effects of sweep on baseline the flow over the model. The second section describes sweep effects on the controlled incompressible flow. The Reynolds number, the excitation frequency, magnitude and location of introduction, as well as the effect of steady mass transfer, are all considered.

Effects of Sweep on the Baseline Flow

Effect of sweep on the baseline and on the controlled flow were studied by rotating the model to a mild sweep angle of $\Lambda = 30$ deg and repeating the same baseline and controlled flow conditions as in the two-dimensional, unswept, configuration.[7] It was found that the Reynolds number has a very weak effect on the model mean and fluctuating pressure distributions (Fig. 4), similar to the two-dimensional flow effect. Note that C_p [solid lines, left-hand side (LHS) ordinate in Fig. 4] is calculated as for two-dimensional flow, and x is measured in the direction perpendicular to the reference leading edge. The same pressure orifices were used to measure the wall pressures, and the x/c location is maintained because the major direction of the attached flow development is assumed to be along the chord, regardless of the sweep angle.

The spanwise distribution of C_p was monitored, and the results for three Reynolds numbers are presented in Fig. 5. Note that $z'/c \equiv r \sin\varphi$, where r is the radial distance between a pressure tap and the center of the turntable, located at $x/c = 0.5$ and $z = 0$, and φ is the angle between r and the $z = 0$ axis. The $z' = 0$ axis is the midpoint between the swept end plates, and it coincides with the freestream direction. The data presented in Fig. 5 show an almost spanwise uniform C_p distribution over the range $-0.3 < z'/c < 0.4$ (where the streamwise row of pressure taps are located, as indicated by the arrow between the two vertical lines on Fig. 5). The deviations from spanwise uniformity are observed to be a weak acceleration along the leading edge [$x/c = 0$, $\Delta C_p/\Delta(z'/c) = -0.08$] and a weak deceleration along the trailing edge [$x/c = 0.95$, $\Delta C_p/\Delta(z'/c) = 0.19$] at all Reynolds numbers considered. An almost perfect spanwise uniformity can be seen at $x/c = 0.49$. Future three-dimensional numerical simulations should be capable of reproducing the small deviation from spanwise uniformity, undesirable as it is.

The effect of sweep on the efficacy of active separation control was studied over a flapped NACA 0018 airfoil at low Reynolds numbers.[17] Various scaling laws were proposed, and the effectiveness of separation control using periodic excitation was demonstrated at swept flow conditions. We shall attempt to apply some of the scaling laws to the baseline flow and subsequently will apply them to the controlled flow as well. Clearly, the scaling for the Reynolds number could not be tested using the present setup and the available data (i.e., surface pressures only), which showed no R_c sensitivity (i.e., Figs. 4 and 5).

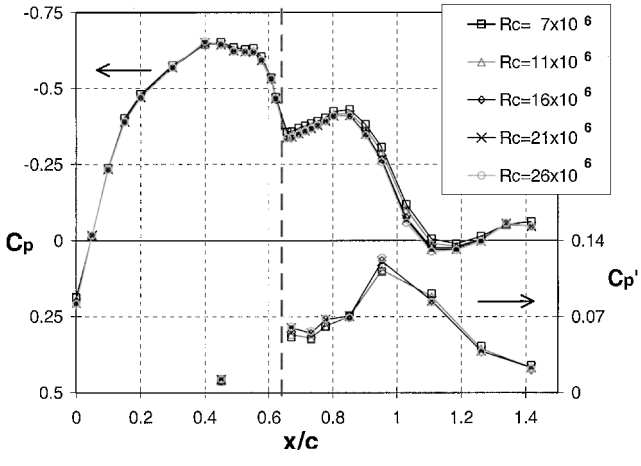

Fig. 4 Mean and fluctuating model pressures at $\Lambda = 30$ deg, $M = 0.25$; R_c indicated in legend. Vertical thick broken line indicates the $x/c = 0.64$ slot location.

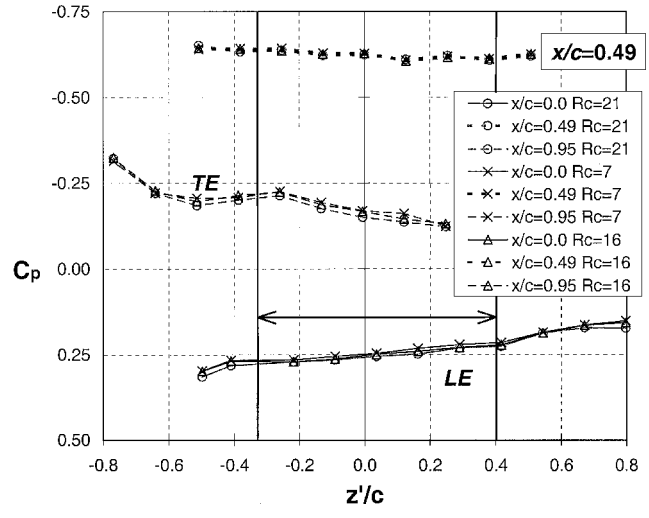

Fig. 5 Spanwise distribution of the model C_p, $\Lambda = 30$ deg, $M = 0.25$; R_c in millions. Two vertical ——, indicate range of streamwise pressure taps.

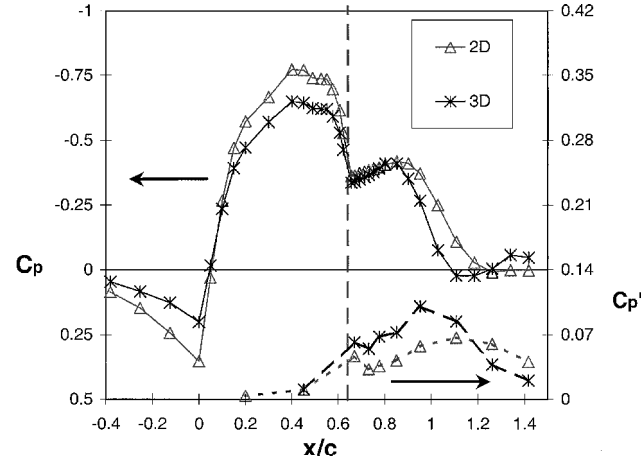

Fig. 6 Comparison of baseline pressure distributions for 0- and 30-deg sweep angles, $M = 0.25$, $R_c = 16 \times 10^6$. Vertical thick – – –, indicates $x/c = 0.64$ slot location.

The effect of sweep on the model baseline pressures is shown in Fig. 6, which compares two- ($\Lambda = 0$) and three-dimensional ($\Lambda = 30$ deg) mean and fluctuating pressure distributions. In agreement with the reduction of the dynamic pressure along the chord of the swept model, according to $q_{3D} = q_{2D} \cos^2 \Lambda$, the magnitude of the C_p (LHS ordinate in Fig. 6, solid lines) is reduced over the attached region of the model at the swept flow condition. The flow separates at $x/c \approx 0.65$, regardless of the sweep angle, and at about the same C_p as in the two-dimensional flow. The two pressure distributions are almost identical from the separation point to $x/c \approx 0.85$. A small difference can be noted in the form of stronger flow acceleration above the bubble in the swept flow, which is indicative of enhanced spreading of the shear layer as a result of enhanced mixing. Moreover, the pressure recovery above the bubble, as the flow turns to the surface, is also stronger at the swept condition, and reattachment therefore occurs upstream of the two-dimensional reattachment. While the two-dimensional flow reattaches at $x/c \approx 1.2$, the swept flow reattaches at $x/c \approx 1.05$ (note that 1.05/cos 30 deg = 1.21). The fluctuating pressure distributions [broken line, right-hand side (RHS) ordinate in Fig. 6] show an even

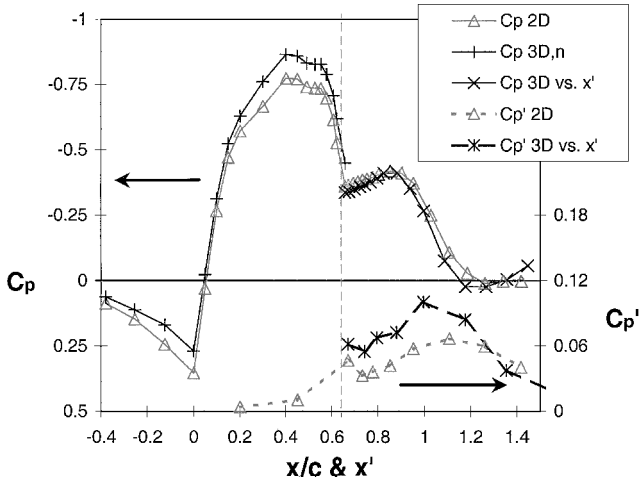

Fig. 7 Scaling of baseline pressure distributions for 0- and 30-deg sweep angles, $M = 0.25$, and $R_c = 16 \times 10^6$; see text for notation.

more dramatic difference between the two- and three-dimensional flows. The C'_p values immediately downstream of separation (i.e., $x/c \approx 0.67$) are amplified in the swept flow, and $C'_{p\,\max}$ is 50% larger than in the two-dimensional flow. The forward motion of $C'_{p\,\max}$ in the swept flow is in agreement with the upstream motion of the reattachment point, as evaluated from the mean C_p. The pressure fluctuations in the three-dimensional flow are lower than their two-dimensional counterparts downstream of reattachment, as seen in two-dimensional flow where reattachment moved forward because of effective control. Clearly, scaling the swept C_{p3D} and C'_{p3D} by a single factor, that is, $\cos^2 \Lambda$, would not collapse the two pressure distributions that are presented in Fig. 6. An alternative simple scaling that subdivides the flow into two regions is suggested: the attached flow C_p (i.e., $x/c < 0.64$), which is normalized by (the traditional) $\cos^2 \Lambda$, and the separated flow region (i.e., $x/c > 0.65$), where the chord is normalized by $\cos \Lambda$. The latter scaling assumes that the flow develops along the external flow direction. The result of this scaling is presented in Fig. 7. It can be observed that the scaling for the attached flow is only partially successful. It undercorrects at $x/c < 0$ and overcorrects at $0.2 < x/c < 0.6$. This disagreement with the conventional scaling cannot be attributed to poor simulation of "infinite" swept flow because the spanwise uniformity is very good at both the LE and midchord regions (Fig. 5). The scaling for the separated and reattached flow (i.e., $x/c > 0.65$) is to plot C_p vs $x/(c \cos \Lambda)$, and this collapses the mean pressure distributions over the bubble very well (solid lines, LHS ordinate in Fig. 7). The location of $C'_{p\,\max}$ (broken lines, RHS ordinate in Fig. 7) for both sweep angles became closer, but the differences in the level of C'_{p3D} vs its two-dimensional counterpart remained. It was shown[18] that the spanwise velocity fluctuation (w') grows very rapidly under an adverse pressure gradient in three-dimensional flow, and the magnitude of w' is similar to that of u' as incipient separation develops. This is an indication that the total turbulence level in three-dimensional separation would be larger by a factor of about $\sqrt{2}$ as compared to the turbulence level in two-dimensional flow. The same reference notes that w' is mainly active near the wall, whereas u', which is a remnant of the upstream attached boundary layer, is mainly active above it, and the two layers merge at reattachment. It is believed that the findings just cited present a possible explanation for the evolution of C'_{p3D}, as shown in Fig. 7, in comparison to the two-dimensional flow, even though it is well known that the wall-pressure fluctuations are a result of an integrated effect of the magnitude of the velocity fluctuations and their respective distance from the wall-pressure measurement location.

Controlled Flow over the "Hump" Model

Overview

This section is devoted to a discussion of the controlled flow over the model. Because the baseline flow contains separated flow, there is no attached baseline flow to be used as a reference. Strong suction was applied in order to reattach the two-dimensional flow at low Mach numbers,[8] and it was used here again to study fully attached three-dimensional flow and examine various scaling laws. Thereafter, periodic excitation was used to gradually control the separation bubble and eliminate it. The parameters that were modified during the test are the frequency and the amplitude of the periodic excitation, the magnitude of the steady mass flux through the slot, as well as the effects of the Reynolds number, were also studied. The spanwise uniformity of the mean wall pressures was found to be very good and generally improved with the application of periodic excitation, regardless of the sweep angle. The effect that the thickness of the turbulent boundary layer upstream of and on the model has on the baseline and on the controlled three-dimensional flow is small and will not be discussed here (see Ref. 7 for a detailed discussion).

Swept Controlled Flow

The swept baseline flow contains a large turbulent separation bubble, as in the two-dimensional flow. Therefore, steady suction or blowing was applied to reattach the flow to the surface of the model gradually. The effectiveness of steady mass flux in modifying the flow is compared in the two- and three-dimensional flows. Steady suction was applied from the $x/c = 0.59$ slot, and the effects on the moment (LHS ordinate) and form drag (RHS ordinate) coefficients are shown in Fig. 8 for $\Lambda = 0$ and 30 deg. The data indicate that the gradual reduction in C_{dp} and the concomitant increase in C_m do not deteriorate for the swept flow, especially for $c_\mu > 0.05\%$.

The data shown in Fig. 9 compare the effectiveness of steady suction and periodic excitation in modifying the form drag on the model at the two sweep angles when control was applied this time from the $x/c = 0.64$ slot. Note the increased effectiveness when the control is applied from the $x/c = 0.64$ slot, compared to its effectiveness when applied from the $x/c = 0.59$ slot (Fig. 8) regardless of the nature of the momentum transfer (i.e., steady or oscillatory). The form-drag data, shown in Fig. 9, indicate that for steady suction as well as for periodic excitation the drag reduction is larger in the swept flow, but the rate of drag reduction is smaller. The C_p data of $F^+ = 2$ and $\Lambda = 0$ deg (Fig. 9) agree very well with the lower F^+ data (not shown), whereas the swept flow data at $F^+ = 2$ show a different trend. It reduces the drag in a more significant manner for low $\langle c_\mu \rangle$ and less for higher $\langle c_\mu \rangle$. This does not happen at lower F^+, as will be shown in Fig. 11.

Figure 10 compares controlled pressure distributions with suction $c_\mu = 0.5\%$ applied from the $x/c = 0.64$ slot for $\Lambda = 0$ and 30 deg. The form drag corresponding to both pressure distributions is nullified by this level of suction (Fig. 9). Note that the swept mean pressure coefficients (LHS ordinate) are scaled according to the

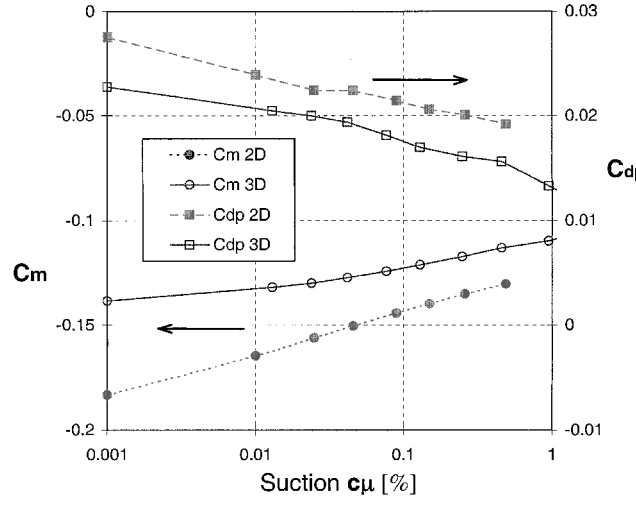

Fig. 8 Effect of sweep on the effectiveness of steady suction as indicated by the moment and form-drag coefficients vs the suction momentum coefficient, $M = 0.25$, $R_c = 21 \times 10^6$, and $x/c = 0.59$ slot.

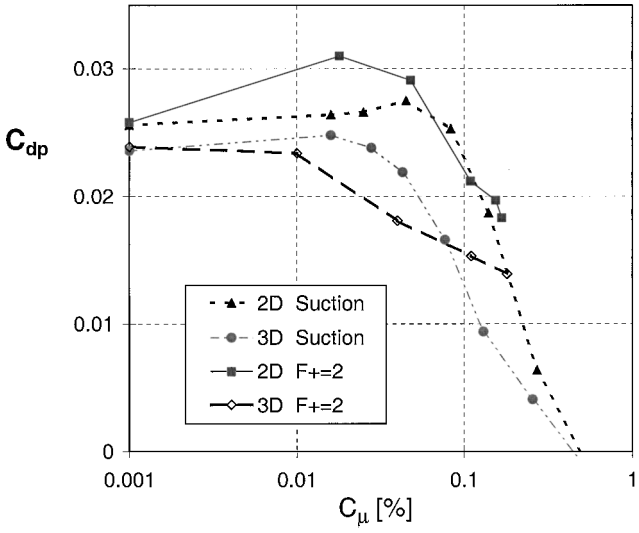

Fig. 9 Effect of sweep on the form-drag coefficient using steady suction (with $F^+ = 0$) or periodic excitation (with $c_\mu = 0$) for control, $M = 0.2$, $R_c = 17.5 \times 10^6$, and $x/c = 0.64$ slot.

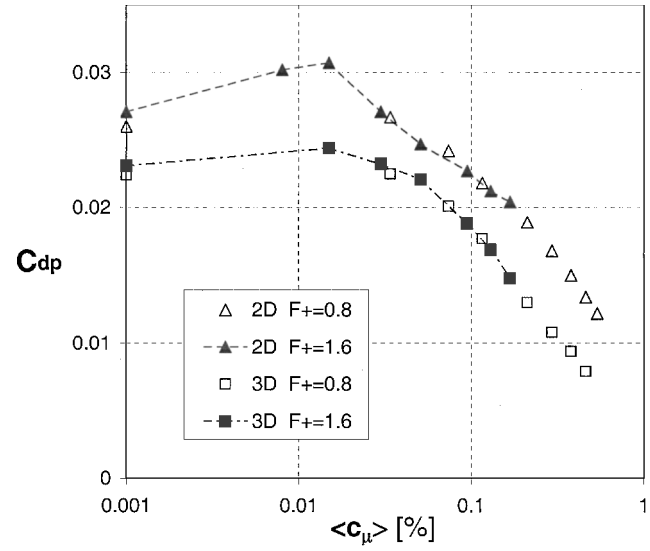

Fig. 11 Effect of sweep on form-drag reduction using $F^+ = 0.8$ and 1.6 for control, $M = 0.25$, $R_c = 16 \times 10^6$, $x/c = 0.64$ slot, and $c_\mu = 0$.

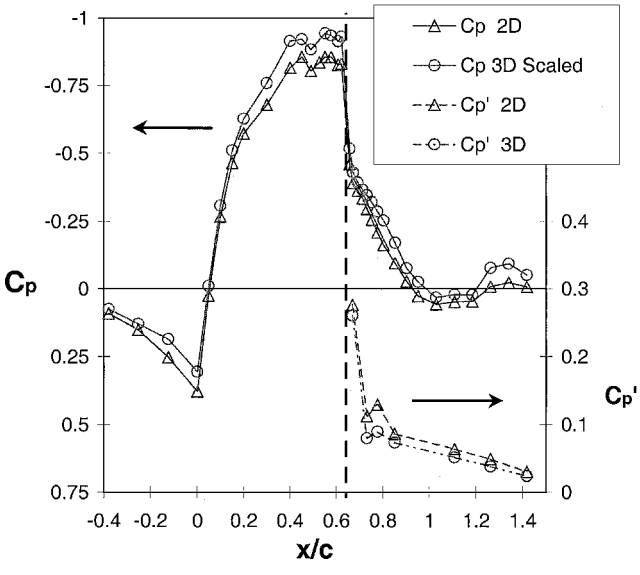

Fig. 10 Effect of sweep on the conventionally scaled C_p using steady suction for control, $M = 0.25$, $R_c = 21 \times 10^6$, vertical dashed broken line indicates $x/c = 0.64$ slot, $c_\mu = -0.5\%$.

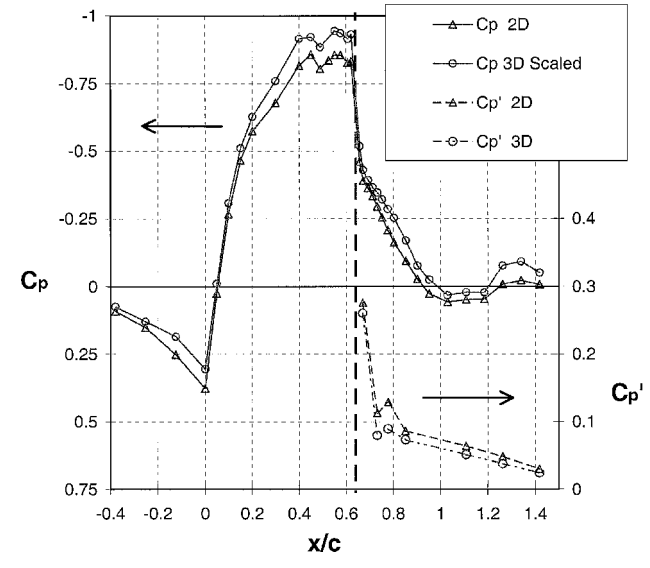

Fig. 12 Effect of sweep on the scaled mean C_p and fluctuating C_p (RHS ordinate) using $F^+ = 2$ and $\langle c_\mu \rangle = 0.2\%$ for control, $M = 0.25$, $R_c = 17.6 \times 10^6$, $x/c = 0.64$ slot, and $c_\mu = 0$.

convention $C_p = C_{p3D}/\cos^2 \Lambda$. The data clearly show that suction at $c_\mu = 0.5\%$ has a comparable effect on the mean and fluctuating flow regardless of the sweep angle and that the conventional scaling works very well for this mostly attached flow. The model surface-pressure fluctuations (C'_p, RHS ordinate) are in very good agreement without any scaling, and so if q_{3D} should be used to scale C'_{p3D} the conclusion would be that it increased by a third in comparison to its two-dimensional counterpart, in agreement with the higher C'_{p3D} measured on the baseline three-dimensional separation bubble.

Figure 11 presents the form drag variation at the two sweep angles as a result of the application of periodic excitation using $F^+ = 0.8$ and 1.6 with increasing $\langle c_\mu \rangle$. Note that the baseline form drag is presented for $\langle c_\mu \rangle = 0.001\%$, for both sweep angles. The sensitivity to F^+ is weak, regardless of the sweep. While at $\Lambda = 0$ deg, periodic excitation with $\langle c_\mu \rangle < 0.02\%$ increases the form drag; at $\Lambda = 30$ deg periodic excitation at $\langle c_\mu \rangle < 0.02\%$ is almost neutral. The effectiveness of periodic excitation using $\langle c_\mu \rangle > 0.02\%$ in reducing the form drag is similar regardless of the sweep angle.

Figure 12 compares pressure distributions with periodic excitation that is applied from the $x/c = 0.64$ slot using $\langle c_\mu \rangle = 0.2\%$ and $F^+ = 2$. Note that the scaling for the swept C_p (i.e., $C_p = C_{p3D}/\cos^2 \Lambda$) collapses the two data sets very well, indicating again that this scaling works well also for partially attached flow. The two- and three-dimensional fluctuating wall pressures (C'_p, RHS ordinate) are in good agreement, without any scaling, consistent with the current findings for reattached flow using steady suction (i.e., that the sweep enhances the separated flow instability). Because the dynamic pressure at the swept flow condition was reduced according to $q_{3D} = q_{2D} \cos^2 \Lambda$, it was suggested[17] that the integral parameters (including the form drag) for the swept flow should scale according to $1/\cos^2 \Lambda$. The swept flow data of Figs. 9 and 11 are replotted in Figs. 13 and 14 when the form drag and the momentum coefficients are scaled according to $C_{dp3D} = C_{dp2D}/\cos^2 \Lambda$ and $C\mu_{3D} = C\mu_{2D}/\cos^2 \Lambda$. The data clearly show that when the control overcomes the massive separation at the lee side of the model, using steady suction with $C_\mu > 0.1\%$ or periodic excitation with $C_\mu > 0.2\%$, the conventional scaling works very well. As long as the flow encloses a massively separated flow region, the conventional three-dimensional scaling fails to collapse the data to a single curve. This is in agreement with the finding that the conventional scaling fails to collapse the pressure distributions that are associated with the bubble.

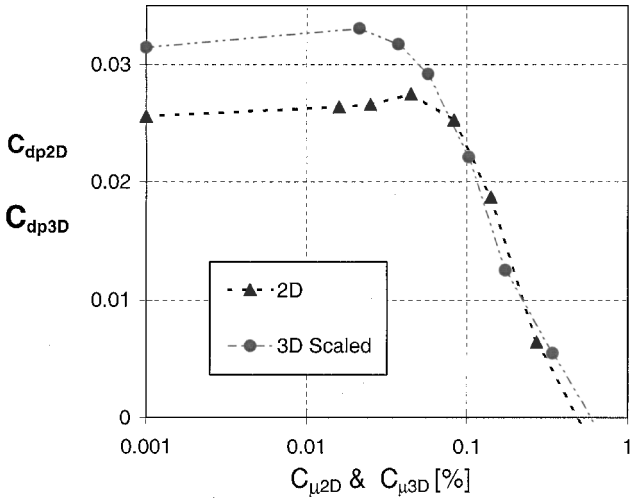

Fig. 13 Effect of sweep on the scaled form drag using steady suction for control, $M = 0.25$, $R_c = 21 \times 10^6$, and $x/c = 0.64$ slot.

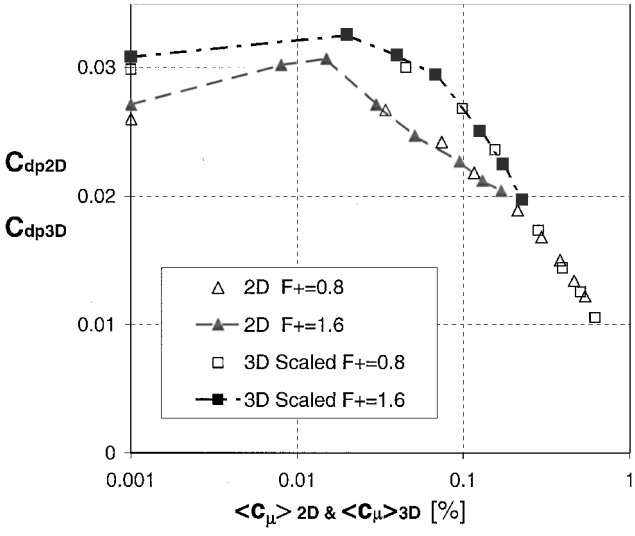

Fig. 14 Effect of sweep on the scaled form drag using $F^+ = 0.8$ and 1.6 for control, $M = 0.25$, $R_c = 16 \times 10^6$, $x/c = 0.64$ slot, and $c_\mu = 0$

IV. Conclusions

Active separation control was applied to a carefully documented baseline flow at high Reynolds numbers. This paper concentrates on effects of mild sweep on the baseline and on the controlled flow. The baseline flow boundary layers are turbulent so that laminar-turbulent transition does not baffle the data trends caused by the active separation control. The Reynolds number has a very weak effect on the model pressure distributions, regardless of the sweep angle.

The effectiveness of the excitation slot located at $x/c = 0.64$ is significantly higher than that of the slot located at $x/c = 0.59$. This is because the magnitude of the excitation decays considerably in the attached region of the boundary layer, because separation takes place at $x/c \approx 0.65$ in the two-dimensional as well as in the swept flow.

The spanwise uniformity of the wall pressures, at unswept flow conditions, was found to be very good and improved as the separation was controlled. The swept flow did not differ considerably from "infinitely" swept flow conditions. Steady as well as periodic control improved the spanwise uniformity at the lee side of the model.

It was found that sweep shortens the bubble and significantly increases the level of the wall-pressure fluctuations upstream of reattachment, in agreement with other experimental data for incipient three-dimensional separation. The attached flow boundary layer develops in a direction perpendicular to the leading edge and scales, as expected, with $1/\cos^2 \Lambda$ while the separated shear layer develops along the freestream direction and scales with $x' = x/\cos \Lambda$, where x is in the direction of the freestream.

Active control using periodic excitation is comparable to steady suction and significantly more effective than steady blowing, as long as the modification of the integral parameters is considered. The efficacy of frequencies with $F^+ \approx 1$ to reattach separated flow is maintained in the three-dimensional flow. The form drag and the momentum coefficients of the control input scale according to the conventional swept flow scaling (i.e., $1/\cos^2 \Lambda$) when the flow is mostly attached.

Acknowledgments

The experiment was performed while the first author held a National Research Council—NASA Langley Research Center research associateship. The authors would like to thank the following individuals for their substantial support of the research program: W. L. Sellers, III; M. J. Walsh; R. D. Joslin; R. W. Wlezien; J. F. Barthelemay; A. McGowen, manager "Aircraft Morphing" program, Airframe systems; B. L. Berrier; L. D. Leavitt; B. K. Stewart; G. C. Hilton; M. K. Chambers; L. Harris, Jr.; P. I. Tiemsin; J. Knudsen; P. T. Bauer; J. Thibodeaux; S. G. Flechner; J. T. Kegelman; and many other NASA employees and contractors and to D. Greenblatt for reviewing the manuscript.

References

[1]Betz, A., "History of Boundary Layer Control in Germany," *Boundary Layer and Flow Control*, Vol. 1, edited by Lachman, Pergamon Press, London, 1961, p. 2.

[2]Nishri, B., and Wygnanski, I., "The Effect of Periodic Excitation on Turbulent Flow Separation from a Flap," *AIAA Journal*, Vol. 36, No. 4, 1998, pp. 547–556.

[3]Seifert, A., Bachar, T., Koss, D., Shepshelovich, M., and Wygnanski, I., "Oscillatory Blowing, a Tool to Delay Boundary Layer Separation," *AIAA Journal*, Vol. 31, No. 11, 1993, pp. 2052–2060.

[4]Seifert, A., Darabi, A., and Wygnanski, I., "On the Delay of Airfoil Stall by Periodic Excitation," *Journal of Aircraft*, Vol. 33, No. 4, 1996, pp. 691–699.

[5]Seifert, A., and Pack, L. G., "Oscillatory Control of Separation at High Reynolds Numbers," *AIAA Journal*, Vol. 37, No. 9, 1999, pp. 1062–1071.

[6]Seifert, A., and Pack, L. G., "Oscillatory Control of Shock-Induced Separation," *Journal of Aircraft*, Vol. 38, No. 3, 2001, pp. 464–472; also AIAA Paper 99-0925, Jan. 1999.

[7]Seifert, A., and Pack, L. G., "Active Flow Separation Control on a Wall-Mounted Hump at High Reynolds Numbers," *AIAA Journal*, Vol. 40, No. 7, 2002, pp. 1363–2372; also AIAA Paper 99-3403, June 1999.

[8]Seifert, A., and Pack, L. G., "Effects of Compressibility and Excitation Slot Location on Active Separation Control at High Reynolds Numbers," part of AIAA Paper 2000-0410, Jan. 2000; *Journal of Aircraft*, Vol. 40, No. 1, 2003, pp. 120–126.

[9]McLean, J. D., Crouch, J. D., Stoner, R., Sakurai, C. S., Seidel, G. E., Feifel, W. M., and Rush, H. M., "Study of the Application of Separation Control by Unsteady Excitation to Civil Transport Aircraft," NASA/CR-1999-209338, June 1999, p. 64.

[10]Lighthill, M. J., "A New Method of Two-Dimensional Aerodynamic Design," Aeronautical Research Council, R&M 2112, London, April 1945.

[11]Glauert, M. B., "The Design of Suction Aerofoils with a Very Large C_L-Range," Aeronautical Research Council, R&M 2111, London, Nov. 1945.

[12]Glauert, M. B., Walker, W. S., Raymer, W. G., and Gregory, N., "Wind-Tunnel Tests on a Thick Suction Aerofoil with a Single Slot," Aeronautical Research Council, R&M 2646, London, Oct. 1948.

[13]Goldschmied, F. R., "Airfoil Static-Pressure Thrust: Flight-Test Verification," 1988 AIAA Aircraft Design and Operating Meeting: Applied Aerodynamics Area, AIAA Paper 88, 1988.

[14]Murthy, A. V., Johnson, C. B., Ray, E. J., Lawing, P. L., and Thibodeaux, J. L., "Studies of Sidewall Boundary Layer in the Langley 0.3-Meter Transonic Cryogenic Tunnel with and Without Suction," NASA-TP-2096, 1983.

[15]Ladson, C. A., and Ray, E. J., "Evolution, Calibration, and Operational Characteristics of the Two-Dimensional Test Section of the Langley 0.3-Meter Transonic Cryogenic Tunnel," NASA-TP-2749, 1987.

[16]Rallo, R. A., Dress, D. A., and Siegle, H. J. A., "Operating Envelope Charts for the Langley 0.3-Meter Transonic Cryogenic Wind Tunnel," NASA-TM-89008, 1986.

[17]Naveh, T., Seifert, A., Tumin, A., and Wygnanski, I., "Sweep Effect on the Parameters Governing the Control of Separation by Periodic Excitation," *Journal of Aircraft*, Vol. 35, No. 3, 1998, pp. 510–512.

[18]Van der Berg, B., and Elsenaar, A., "Measurement in a Three-Dimensional Incompressible Turbulent Boundary Layer in an Adverse Pressure Gradient Under Infinite Swept Wing Conditions," N.L.R. TR 72092 U, 1972.